Neurobiology of Disease 190 (2024) 106382

Contents lists available at ScienceDirect

Neurobiology of Disease

journal homepage: www.elsevier.com/locate/ynbdi

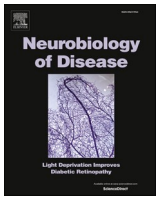

Reproducible network changes occur in a mouse model of temporal lobe epilepsy but do not correlate with disease severity

Isotta Rigoni [a,*], Guru Prasad Padmasola [b,c], Laurent Sheybani [a,c], Karl Schaller [d], Charles Quairiaux [b], Serge Vulliemoz [a]

[a] EEG and Epilepsy unit, Department of Neuroscience, University Hospital and Faculty of Medicine of Geneva, University of Geneva, Geneva, Switzerland
[b] Department of Basic Neuroscience, Faculty of Medicine, University of Geneva, Geneva, Switzerland
[c] Department of Clinical and Experimental Epilepsy, UCL Queen Square Institute of Neurology, London, UK
[d] Department of Neurosurgery, University Hospital and Faculty of Medicine of Geneva, Geneva, Switzerland

ARTICLE INFO

Keywords:
Hippocampal kainate mouse model
Temporal lobe epilepsy
Functional connectivity
EEG

ABSTRACT

Studying the development of brain network disruptions in epilepsy is challenged by the paucity of data before epilepsy onset. Here, we used the unilateral, kainate mouse model of hippocampal epilepsy to investigate brain network changes before and after epilepsy onset and their stability across time.

Using 32 epicranial electrodes distributed over the mouse hemispheres, we analyzed EEG epochs free from epileptic activity in 15 animals before and 28 days after hippocampal injection (group 1) and in 20 animals on two consecutive days (d28 and d29, group 2). Statistical dependencies between electrodes were characterized with the debiased-weighted phase lag index. We analyzed: a) graph metric changes from baseline to chronic stage (d28) in group 1; b) their reliability across d28 and d29, in group 2; c) their correlation with epileptic activity (EA: seizure, spike and fast-ripple rates), averaged over d28 and d29, in group 2.

During the chronic stage, intra-hemispheric connections of the non-injected hemisphere strengthened, yielding an asymmetrical network in low (4–8 Hz) and high theta (8–12 Hz) bands. The contralateral hemisphere also became more integrated and segregated within the high theta band. Both network topology and EEG markers of EA were stable over consecutive days but not correlated with each other.

Altogether, we show reproducible large-scale network modifications after the development of focal epilepsy. These modifications are mostly specific to the non-injected hemisphere. The absence of correlation with epileptic activity does not allow to specifically ascribe these network changes to mechanisms supporting EA or rather compensatory inhibition but supports the notion that epilepsy extends beyond the sole repetition of EA and impacts network that might not be involved in EA generation.

1. Introduction

Epilepsy is a neurological disease affecting nearly 1% of the worldwide population characterized by the occurrence of recurrent seizures and interictal epileptiform discharges (IEDs) on electroencephalography (EEG) (Fisher et al., 2014). Epilepsy is now unanimously recognized as a brain network disorder (Bartolomei et al., 2017), meaning that even "focal" epilepsies such as temporal lobe epilepsy (TLE) involve pathological interactions between different brain regions. Both seizures and IEDs -and their network signatures- are widely studied (Carboni et al., 2019; Rigoni et al., 2023a; Terry et al., 2012; van Mierlo et al., 2019) as they are clinically useful to diagnose and characterize the brain disorder. However, their unpredictability and variability are a strong motivation to further investigate abnormalities in background activity that could help better understand the pathological mechanisms and could represent potential diagnostic and prognostic biomarkers, especially considering that >40% of clinical EEG do not present epileptiform abnormalities (Geut et al., 2017; King et al., 1998; Wirrell, 2010).

EEG studies showed that the IED-free interictal activity of patients with TLE is characterized by different connectivity patterns than that of healthy controls, such as higher network integration and segregation (Carboni et al., 2020; Coito et al., 2019; Rigoni et al., 2023b; Verhoeven et al., 2018), suggesting that even resting-state non-epileptiform brain activity contains important information with clinical validity.

* Corresponding author.
E-mail address: isotta.rigoni@unige.ch (I. Rigoni).

https://doi.org/10.1016/j.nbd.2023.106382
Received 11 October 2023; Received in revised form 27 November 2023; Accepted 13 December 2023
Available online 17 December 2023

Alterations of interictal brain networks were found also in functional magnetic resonance imaging (fMRI) studies (de Campos et al., 2016; Kay et al., 2013), although the IED contribution to the altered connectivity cannot be controlled for. Furthermore, fMRI measures blood oxygenation changes rather than neuronal electrical brain activity. Therefore, it is not trivial to perform comparisons across both modalities.

Animal models are crucial to study aspects of diseases that are hard if not impossible to investigate in humans, such as the comparison between brain activity before and after epilepsy onset. Connectivity studies in rodents with epilepsy are mostly carried out with fMRI and show interictal changes that resemble those observed in humans. Most studies point at a higher level of brain connectivity, integration and segregation in epileptic animals (Bertoglio et al., 2019; Li et al., 2021; Singh et al., 2017), and to their relationship with seizure frequency (Bertoglio et al., 2019; Christiaen et al., 2019, 2020; Samiee et al., 2018). Only one previous study from our group (Słowiński et al., 2019) used EEG to derive and investigate specifically IED-free interictal brain networks and found increasing network asymmetry in favor of the hemisphere contralateral to the lesion. Here, we aimed at expanding the characterization of networks based on interictal background activity between the occurrence of IED.

Discrepancies in connectivity studies exist in animal (Christiaen et al., 2019, 2020), as they do in human research (Slinger et al., 2021). Considering these controversies, we also wanted to evaluate the repeatability of network metrics in a mouse model of TLE, the leading cause of pharmacoresistant epilepsy in human adults. Here, we study within-animals brain network changes in the intrahippocampal kainate (KA) mouse model, which is the most widely used and reliable model for unilateral temporal lobe epilepsy (Arabadzisz et al., 2005; Lévesque and Avoli, 2016). Following KA-induced status epilepticus, this model is characterized by the development of unilateral hippocampal sclerosis representative of the most common lesion in human TLE. This contrasts with other models using intraperitoneal (i.p.) KA or pilocarpine models that lead to bilateral sclerosis and various cortical lesions (Rusina et al., 2021). Within a few weeks, a focal epileptic disease develops with frequent ictal discharges generated in the KA-injected hippocampus, i.e., the epileptic focus, and less frequent secondarily tonic-clonic seizures (Lisgaras and Scharfman, 2022; Paschen et al., 2020; Riban et al., 2002; Sheybani et al., 2018). Although seizures start in and mostly remain within the KA-injected hippocampal region, large-scale functional alterations have also been described, with the expression of IEDs invading both hemispheres, comprising neocortical areas (Sheybani et al., 2018, 2019).

We hypothesized that: 1) the epileptogenic lesion would induce changes in the animals' brain network, observable as increase in global, hemispheric, and nodal measures of integration and segregation; 2) these network changes -and the frequency of epileptiform abnormalities in EEG recordings- would be reproducible at the chronic stage; 3) these network changes would correlate with the severity of the epilepsy.

2. Materials and methods

2.1. Animals

Twenty-nine male C57BL/6j mice (Charles River) were included in this study. All animals were around 10–11 weeks old when they entered the protocol. EEG was recorded at the baseline (d0), i.e. before the KA injection (d1), and on two consecutive days during the chronic phase (d28 and d29, see timeline in Fig. 1.b), which is defined as the timepoint when the majority of animals develop spontaneous seizures (Rusina et al., 2021; Sheybani et al., 2018). As not all animals were recorded on every timepoint, animals were split into two groups and were used for different analyses. Group A consisted of $N = 15$ animals that were recorded on d0 and d28 (see Fig. 1.a): these animals were used to test the first hypothesis. Group B consisted of $N = 20$ animals that were recorded on d28 and d29, which were used to test the second and third hypothesis (6 animals belonged also to group A, see Fig. 1.a).

2.2. Surgery

Head-fix surgeries were carried out under injectable anesthesia using a sleep cocktail (Medetomidine (Domitor): 0.5 mg/kg, Midazolam (Dormicum): 5 mg/kg, Fentanyl: 0.05 mg/kg) delivered intraperitoneally. Briefly, as described in detail previously (Sheybani et al., 2018), an aluminum ring-like header was attached to the mouse skull using dental cement, after the skin was reclined. The positions of the EEG electrodes were marked using blue ink. A drop of Loctite was spread over the skull to form a thin layer, then small patches (500 μm) of the

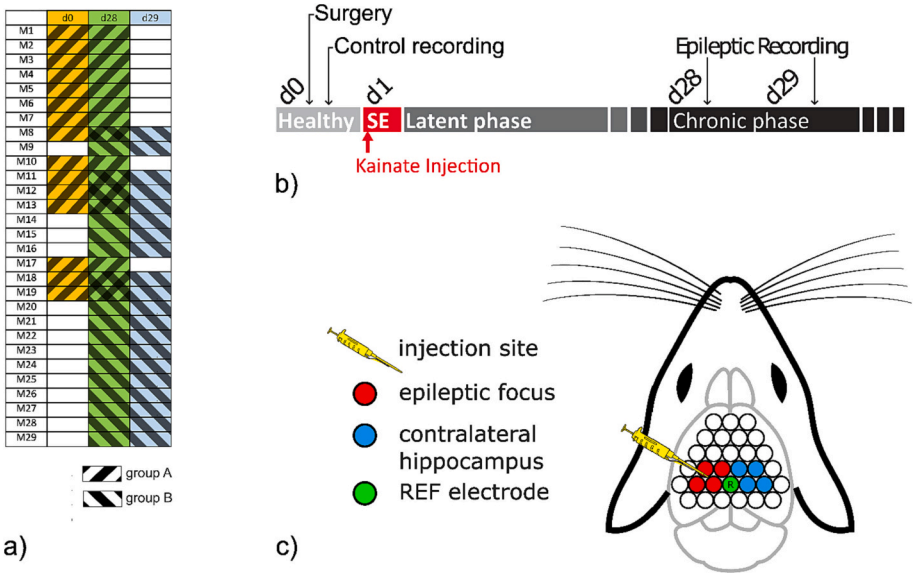

Fig. 1. Study protocol. A) Table representing the distribution of the animals in the two groups. B) Time-frame of surgery, kainate injection and data acquisition. C) Schema of the EEG electrode positioning on the mouse brain, highlighting the injection site (yellow syringe), the epileptic focus (red electrodes, overlying the left hippocampus) and the non-injected hippocampus (blue electrodes). The mouse schema was adapted from scidraw.io (https://zenodo.org/record/3925903#.Y9qN0HbMKUk). (For interpretation of the references to colour in this figure legend, the reader is referred to the web version of this article.)

Loctite were removed by drilling over the electrode marked positions using a nano drill. The center of the aluminum ring-like holder was then filled with protective silicon (kwik-cast, World Precision Instrument), which can be easily removed and replaced to allow access for further injections and recordings. After the procedure, an awake cocktail (Flumazenil (Anexate): 0.5 mg/kg, Atipamezol (Alzane): 2.5 mg/kg, Naloxone: 1.2 mg/kg) was administered subcutaneously before the animal was returned to his cage and placed under a heating light for a brief duration until they were awake. In addition to food and play materials, antibiotics (trimethoprim-sulfamethoxazole, Roche) and anti-inflammatory analgesics (ibuprofen, Vifor, and paracetamol, Bristol-Myers) were delivered in the drinking water. Before administering kainate injections, the animals were given one week to recover and rebuild strength.

2.3. Kainate injection

The KA injection site was marked with ink during the head-fix surgery procedure and the injections were performed one week after the head-fix surgery. Under isoflurane anesthesia, the animal was mounted on the stereotaxic frame and the previously applied kwik-cast removed. Using a dental drill, a 0.3 mm hole was drilled above the injection site. Using a drawn glass capillary (Drummond glass capillaries # 3–000-203 G/X; tip diameter 15 μm), a volume of 70 nl kainic acid (Tocris Bioscience; 5 mM in NaCl 0.9%) was administered at a rate of 10 nl/s into the left dorsal hippocampus (Mediolateral 1.6 mm, Anteroposterior −1.8 mm, Depth 1.9 mm). Within an hour from injection, all animals had a clear status epilepticus that was allowed to self-terminate and that was characterized by rearing and falling with unilateral or bilateral forelimb clonus (stage 3–5 on the Racine scale) (Racine, 1972; Rusina et al., 2021; Sharma et al., 2018). The day when KA injection was performed is referred to as d1.

2.4. EEG recordings and analyses

Epicranial EEG was recorded with 31 stainless-steel electrodes (diameter of 500 μm) covering the entire skull surface as shown in Fig. 1.b and as previously described (Mégevand et al., 2008; Quairiaux et al., 2011; Silachev et al., 2022). Recordings were performed on d0, i.e. the day before the KA injection, and 28 and 29 days after the injection (d28 and d29). During the three to four days preceding the first recording session, all animals were trained to remain in the head-fix position twice a day. The training time was gradually increased from 10 to 30 min. The animals were momentarily sedated with isoflurane anesthesia prior to the recording sessions to allow electrode positioning. The recordings were then carried out once the animals were fully awake and lasted approximately 30–50 min. All recordings were acquired with a Digital Lynx SX (Neuralynx), using a sampling frequency of 4 kHz, with an online band-pass filter of 0.1–2 kHz. An in-house automated MATLAB algorithm was used to detect abnormal pathological activity on the whole recording, as explained in the next paragraph. The recordings were segmented in epochs of 2 s and we discarded those <2 s away from epileptic events (see details below). We visually identified and removed epochs containing artifacts and then randomly selected 50 epochs for analysis. Data were downsampled to 250 Hz and bandpass filtered (1–40 Hz) with a 6th Butterworth filter. Channels with poor signal-to-noise ratio were identified as those with standard deviation (SD) -computed across epochs- exceeding the third quartile by a factor of 2 times the interquartile range. These were replaced by a 'spline' interpolation of the neighboring channels (Perrin et al., 1989). Finally, the epochs were re-referenced to the average and the reference electrode was removed, leaving 30 electrodes for connectivity analyses.

2.5. Identification of epileptiform activity

To quantify epileptiform activities (EA) in a standardized manner and eliminate examiner bias, we used an algorithm-based fast-ripples (FRs) detection method. FR were targeted because they almost systematically override EA during the spikes component (Lévesque et al., 2018; Weiss et al., 2016).

First, FRs are identified on all electrodes using an automated detector previously described in detail (Sheybani et al., 2018; Słowiński et al., 2019) The raw signal (0.1-2 kHz, sampling frequency of 4 kHz) is first filtered between 200 and 550 Hz (2nd order Butterworth filter). FRs are then identified as events with $\geq$4 consecutive oscillations with amplitude 3 times greater than the standard deviation of the 250 ms surrounding baseline. To avoid identifying harmonics of lower frequency activities as FRs, the detector retains only FRs that do not overlap with ripples or high-gamma activity. When two FRs are detected at two distinct sites without phase lag, volume conduction is assumed to have occurred and only the event with the greatest power is preserved. Finally, all detected events are visually validated in filtered and unfiltered data. Then, FRs detected on the electrodes positioned above the epileptic focus (see Fig. 1.b) are used to identify and classify *focal EA*. In the raw non-filtered data, a marker is positioned on the positive peak of the spike waveform associated with each FR and peak-to-peak interspike intervals are calculated to classify epileptic patterns as follows. Discharges neither preceded nor followed by another spike for at least 1 s are classified as isolated spikes (IS). Events with $>$2 successive spikes within a second are further separated according to spike rates and event duration. Events that never display $>$5 spikes/s are named spike trains (STs); the first spike not followed by another for at least one second marks their termination. Events that reach $>$5 spikes/s but do not exceed 10 s are classified as short hippocampal paroxysmal discharges (sHPDs), those that exceed 10 s are classified as ictal hippocampal paroxysmal discharges (iHPDs) and are considered as reminiscent of focal seizures (Sheybani et al., 2018). Electrographic seizures are known to emerge after 2–3 weeks in the kainate model, which is considered as chronic stage of the disease (Arabadzisz et al., 2005; Riban et al., 2002; Sheybani et al., 2018). Here, we therefore allocate all our EEG recordings made after the 4th week (d28 and d29) to the chronic phase of the disease.

FRs occurring on all other electrodes are classified as remote FRs and regarded as *network EA*. A reviewer blind to the animal condition also identified a large-scale type of IEDs that we classify as network IED and that correspond to the previously described generalized spikes (Sheybani et al., 2018). Network IEDs are characterized by a large-scale network and two spiking bursts separated by flattening of the EEG of approximately 250 ms. Note that remote FRs co-occurring with network IEDs were not included in the remote FRs quantification. From now on, the term epileptiform activities (EA) will refer to the ensemble of features described in this paragraph (see Fig. 2). Examples of traces of EA are depicted in Supplementary Fig. S1.

2.6. Connectivity analyses

We quantified the statistical dependencies between the 30 electrodes with the debiased weighted phase lag index (dwPLI). The Fourier transform was calculated using multitapers based on the Slepian sequence with a 2 Hz smoothing box. The resulting functional connectivity (FC) matrix (30 $\times$ 30 $\times$ 81, where 30 is the number of EEG channels and 81 is the number of frequency bin spacing from 1 to 40 Hz) was averaged across the different frequency bands. This yielded five average matrices for each animal on each recording day: delta (1–4 Hz), theta or "low-theta" (4–8 Hz), alpha "or high-theta" (8–12 Hz), beta (12–30 Hz) and low-gamma (30–40 Hz). EEG preprocessing and connectivity analyses were implemented in MATLAB using the MATLAB-based Fieldtrip toolbox (Oostenveld et al., 2011).

2.7. Graph analyses

The FC matrices describe the brain as a network where the nodes are the different brain regions, and the edges are their statistical de-

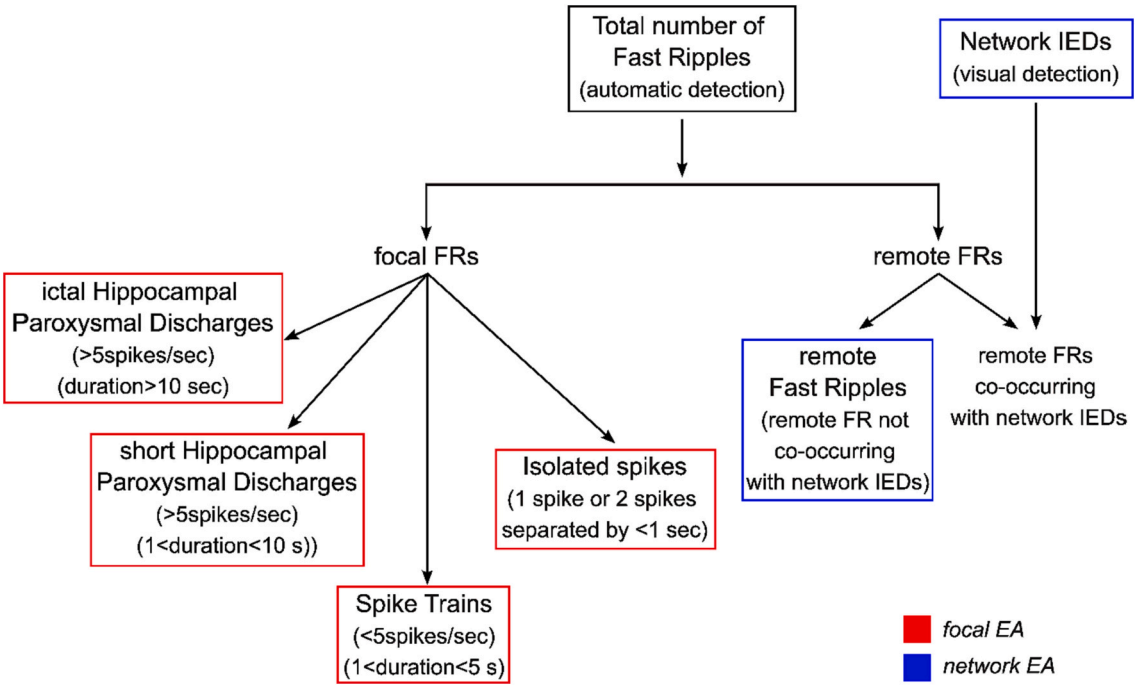

Fig. 2. Classification of epileptiform activities. Focal (red boxes) and network (blue boxes) epileptiform activities are identified from the automatically detected fast ripples (FR) and the visually-detected network IEDs. The EA retained for correlation analyses are those surrounded by black, red and blues boxes. (For interpretation of the references to colour in this figure legend, the reader is referred to the web version of this article.)

pendencies. To fully characterize it, we extracted graph measures that describe the integration (efficiency, E), the segregation (clustering coefficient, CC) and the balance of the specific network (laterality index, LI). We did so at three different levels: global, hemispheric and nodal. The global measures are the average of the nodal ones. Hemispheric measures were computed as global ones, only that the network to which they referred comprised the nodes belonging exclusively to the specific hemisphere and their intra-hemispheric connections (midline electrodes were removed from the computation, see Fig. 1.b). For integration, we extracted the global, the hemispheric and the nodal efficiency (GE, HE and NE respectively), which, at the global level, reflects how efficiently information is propagated and integrated over different nodes. The efficiency of node i, NE_i, was calculated as the average of the inverse of the distance d between node i and all other nodes connected to i (Rubinov and Sporns, 2010):

$$NE_i = \frac{\sum_{j\in N, j\neq i} NE_{ij}}{n-1} = \frac{1}{(n-1)} \sum_{i\neq j\in N} \frac{1}{d_{ij}}$$

As the distance d_{ij} was calculated as the inverse of the connection between nodes i and j, the efficiency of the communication between i and j (NE_{ij}) is inversely proportional to their distance (Latora and Marchiori, 2001). Intuitively, the higher the distance between i and j, the smaller the efficiency in their communication. For segregation, we extracted the global, the hemispheric and the nodal CC (GCC, HCC and CC, respectively), which, at the global level, reflects the level of clustered connections around individual nodes. The clustering coefficient of node i, CC_i, is the fraction of i's neighbors that are also neighbors to each other (Watts and Strogatz, 1998):

$$CC_i = \frac{2t_i}{k_i(k_i-1)}$$

where k_i is the strength of the node (calculated as the sum of all i's edges) and t_i is the number of triangles attached to the node (Rubinov and Sporns, 2010). Lastly, we calculated the LI of the network based on nodal strength as previously proposed (Coito et al., 2015):

$$LI = \frac{\left(\sum_{i\in N, i\in LEFT} k_i - \sum_{i\in N, i\in RIGHT} k_i\right)}{\left(\sum_{i\in N} k_i\right)}$$

where a positive value indicates that the total strength of the nodes in the left hemisphere (ipsilateral to injection) is higher than the total strength of the nodes in the right hemisphere (contralateral) (left>-right), and vice versa. From now on, for the sake of clarity, we will refer to the left and right hemisphere as to the hemisphere ipsilateral and contralateral to the epileptogenic focus.

All measures were extracted with the Brain Connectivity Toolbox (Rubinov and Sporns, 2010).

2.8. Statistical analyses

For group A ($N = 15$), we compared global and hemispheric network metrics (GE, GCC, LI, HE and HCC) at baseline (d0) vs chronic stage (d28) with a two-side Wilcoxon signed rank test. For each metric, we Bonferroni-corrected the p-values for the 5 tests run across frequency bands. For the nodal metrics, NE and NCC, we used a two-side cluster-based permutation test to correct for the 30 electrodes. The latter was implemented with the Fieldtrip toolbox (Oostenveld et al., 2011), using 5000 permutations. To reduce the number of tests, we only looked at the frequency bands that showed differences in the global and hemispheric measures and we Bonferroni-corrected the cluster significance. Furthermore, to investigate if epilepsy *induced* brain asymmetry (rather than just looking at whether asymmetry increased or decreased from d0 to d28) we also tested whether the network was balanced (LI = 0) at baseline and became unbalanced (LI > 0 or LI < 0) at chronic stage. To do so, we used a Wilcoxon test to test if LI was significantly different from zero at d0 and d28, only in those frequency bands where there were differences between LI at d0 and d28. The p-values were Bonferroni-corrected for the 4 tests.

With group B ($N = 20$), we investigated the reproducibility of both

FC and EA at the chronic stage (d28 vs d29). We repeated the analyses described in the previous paragraph for network metrics (GE, GCC, LI, HE, HCC, NE and NCC), and then used correlation analyses to further test the stability of functional connectomes and EA. For the latter step, we averaged the frequency-specific FC matrices across animals and calculated the interclass correlation coefficient (ICC) between the average matrix at d28 with the average matrix at d29. The *p*-values were Bonferroni-corrected for the 5 frequency bands. We also tested the ICC between EA at d28 and d29 (IS, ST, sHPD, iHPD, network IEDs, remote FRs and the total number of all FRs) and Bonferroni-corrected the *p*-values for the number of measures tested (7). The ICC for absolute agreement was calculated with the ICC function (Arash Salarian, 2023) for average (ICC(A,k) for FC matrices) and single measurements (ICC (A,1) for EA) (McGraw and Wong, 1996). Results are reported with 95% confidence intervals (CI).

Finally, as reproducibility results suggested high stability of FC and EA in the chronic state, we looked at the relationship between the average FC and EA values. Specifically, we averaged individual FC matrices across d28 and d29 and re-extracted the global and hemispheric graph measures (GE, GCC, HE, HCC, and LI). Then, we averaged EA across the two consecutive days and tested whether they were related to the graph metrics extracted from the averaged FC matrices. To reduce the number of comparisons we only tested the correlation with those graph measures that significantly changed from d0 to d28 (those that were affected by the epilepsy), and Bonferroni-corrected the *p*-values. A Pearson's or Spearman's correlation test was used, depending on the presence of outliers.

3. Results

3.1. Epileptiform activity

We detected iHPDs events -reminiscent of focal seizures- in 24 out of 29 animals. The remaining 5 animals without recorded iHPDs still presented with clear epileptiform discharges (see Supplementary Tables S1 and S2); lack of iHPDs detection in these animals could be consecutive to the discontinuous nature of our recordings.

3.2. Global and hemispheric measures

Global graph measures, namely GE and GCC, did not show any significant difference between baseline and chronic state. However, at intra-hemispheric level, graph measures changed significantly, but only in the hemisphere contralateral to the epileptogenic focus. Specifically, both high-theta HE and HCC of the contralateral hemisphere increased in the chronic state as compared to baseline ($p = .042$ and $p = .0043$, respectively; see Fig. 3.a). No changes were observed in the intra-hemispheric connections of the injected hemisphere (see Supplementary Fig. S2). The strength LI significantly decreased from d0 to d28, in both low- and high-theta frequency bands ($p = .0006$ and $p = .0021$, respectively), meaning that nodes of the contralateral hemisphere became stronger at the chronic stage (see Fig. 3.b). Furthermore, when testing the lateralization at d0 and d28 separately, we observed that the LI was not significantly different from a zero-median distribution at d0 in any frequency bands, while it was significantly smaller than zero

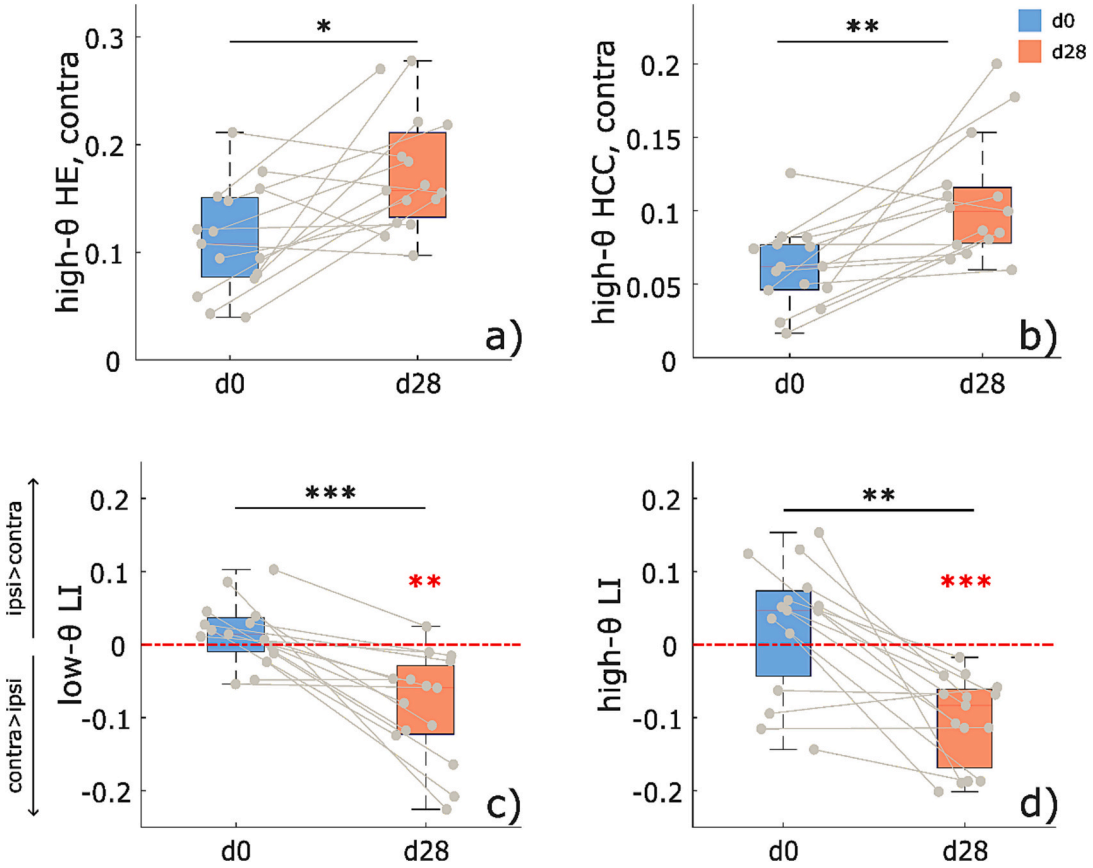

Fig. 3. Hemispheric graph measure results. First row: boxplots of HE (a) and HCC changes (b) from baseline (d0, blue) to chronic stage (d28, red), that occurred only in the contralateral hemisphere. Second row: boxplots of LI changes from d0 to d28, found both in low-theta (c) and high-theta (d) frequency band. The red dotted line represents the zero-median with which all four distributions (LI in low-theta and high-theta, at d0 and d28) were compared. The red asterisks indicate a LI-distribution that is significantly different from zero, i.e. a network that is lateralized and not balanced. All asterisks in the figure represent statistical significance (* for $p < .05$, ** for $p < .01$ and *** for $p < .001$). (For interpretation of the references to colour in this figure legend, the reader is referred to the web version of this article.)

(lateralized toward the contralateral hemisphere) at d28, in both low-theta and high-theta bands ($p = .0017$ and $p = .00024$, respectively; see the red asterisks in Fig. 3.b). Interestingly, while in high-theta it was the nodal strength of the *contralateral* hemisphere that *increased* at d28 (see Supplementary Fig. S3.b), in low-theta it was the nodal strength of the *ipsilateral* hemisphere that *decreased* at d28 (see Fig. S3.a), which both led to an increased lateralization toward the contralateral hemisphere at the chronic stage.

3.3. Nodal measures

When comparing the nodal measures between the two time points in low- and high- theta, the cluster -based permutation test revealed a significant increase of both NE and CC in high-theta from d0 to d28 ($p = .02$ and $p = .014$, respectively). In this frequency range, the effect was most pronounced in electrodes overlying the contralateral hippocampus and occipital cortex (see yellow asterisks in Fig. 4.a.2 and 4.b.2). Although a decrease of both NE and CC can be visually noticed in the occipital part of the ipsilateral hemisphere in low-theta (see Fig. 4.a.1 and Fig. 4.b.1), these were not significant.

3.4. Stability and reproducibility at the chronic stage

When repeating these analyses between d28 and d29, we found no significant difference for any of the network metrics (GE, GCC, LI, HE, HCC, NE and NCC). The specular results of Fig. 3 are reported in Fig. S4. Moreover, we found that networks were significantly lateralized toward the contralateral hemisphere at both d28 and d29, in both low- and high-theta ($p < .01$, see Fig. S4.b). As a further confirmation of the brain network similarity between d28 and d29, when functional connectomes were averaged across animals, high ICC indicating excellent reliability were found in delta ($ICC_{A,k} = 0.96$, $CI_{95} = [0.92\ 0.98]$, $F_{(434,18.4784)} = 33.67$, $p < .001$), low-theta ($ICC_{A,k} = 0.97$, $CI_{95} = [0.97\ 0.98]$, $F_{(434,434.3361)} = 38.96$, $p < .001$), high-theta ($ICC_{A,k} = 0.97$, $CI_{95} = [0.96\ 0.98]$, $F_{(434,\ 425.3896)} = 34.33$, $p < .001$, see Fig. 5.a for an example), beta ($ICC_{A,k} = 0.95$, $CI_{95} = [0.93\ 0.96]$, $F_{(434,\ 69.746)} = 22$ $p < .001$) and low-gamma ($ICC_{A,k} = 0.93$, $CI_{95} = [0.92\ 0.94]$, $F_{(434,434.388)} = 14.46$, $p < .001$) between connectivity values on the two consecutive days. Similarly, a significant ICC indicating good reliability was found for most of the EA between d28 and d29, although, in general, ICC values were lower than those obtained for FC. Specifically, a significant ICC was found for many EA measured on d28 and d29: number of iHPD ($ICC_{A,1} = 0.75$, $CI_{95} = [0.47\ 0.9]$, $F_{(19,16.777)} = 7.99$, $p = .0003$, see Fig. 5.b), total number of FR ($ICC_{A,1} = 0.75$, $CI_{95} = [0.46\ 0.89]$, $F_{(19,19.1685)} = 6.64$, $p = .0004$, see Fig. 5.c), isolated FR ($ICC_{A,1} = 0.74$, $CI_{95} = [0.45\ 0.89]$, $F_{(19,19)} = 6.38$, $p = 0006$), number of network IEDs ($ICC_{A,1} = 0.9$, $CI_{95} = [0.77\ 0.96]$, $F_{(19,19.4748)} = 18.6$, $p = 8.3415e\text{-}08$, see Fig. 5.d), and isolated spikes ($ICC_{A,1} = 0.77$, $CI_{95} = [0.5\ 0.9]$, $F_{(19,19.1406)} = 7.3$, $p = .0002$). No significant ICC was found for sHPD- and spike trains-rate on the two days.

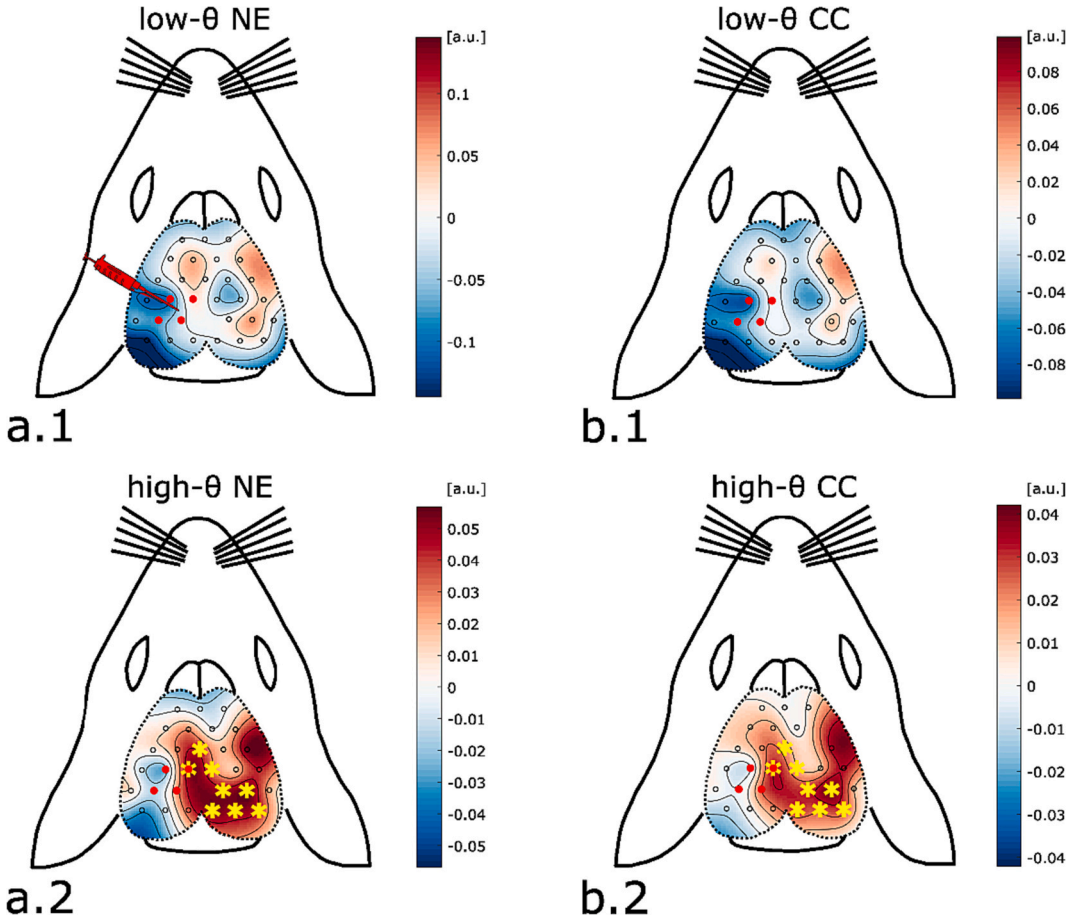

Fig. 4. Nodal graph measure results. Results of cluster-based permutation test run on a) nodal efficiency (NE) and b) clustering coefficient (CC), in 1) low-theta and 2) high-theta frequency bands. The values displayed on the map are the average differences between nodal measures at the chronic stage and baseline. Red/blue values therefore represent an increase/decrease of the specific graph measure from baseline. The electrodes with a yellow star are those that belong to the identified cluster ($p < .01$). The electrodes in red represent the injected hippocampus and the red syringe indicates the KA injection site. Note that the scales used for the plots are different from each other. (For interpretation of the references to colour in this figure legend, the reader is referred to the web version of this article.)

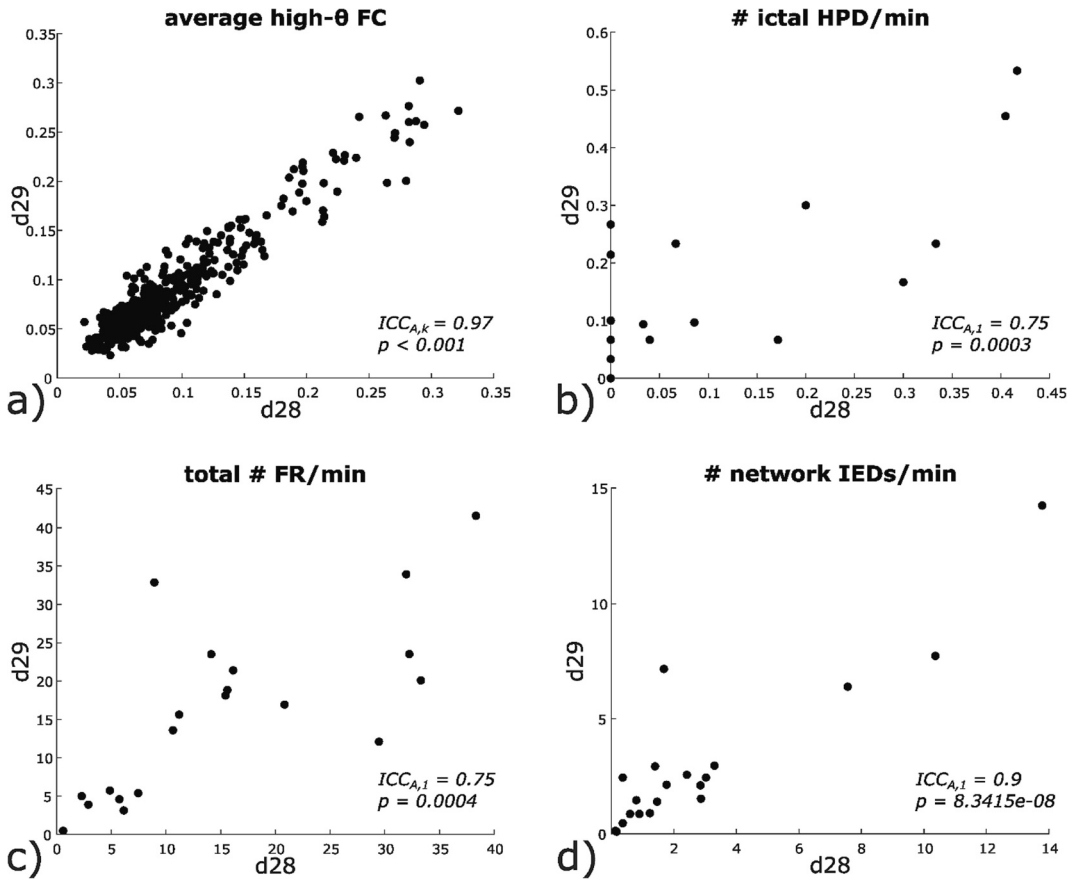

Fig. 5. Reproducibility results in the chronic stage. a) Results of Pearson's correlation analysis on high-theta functional connectivity (FC) matrices, averaged across animals. Each dot is a unique entry of the average matrix, at the specific day. b), c) and d) show some of the results of the correlation analyses run on the EA measured at day 28 and day 29: b) rate of ictal hippocampal paroxysmal discharges (reminiscent of focal seizures); c) total number of FR per minute; d) rate of network IEDs. Note that in b) 5 points are superimposed in [0,0].

3.5. Correlation of network metrics with epileptic activity

Finally, when we correlated the graph metrics extracted from the average FC matrix and the EA averaged over d28 and d29 we did not find any significant results. Correlation analyses were run only for those network metrics that showed a significant change from d0 to d28, namely high-theta right HE and right HCC, and LI in low-theta and high-theta. To visualize this absence of correlation, Fig. 6 shows the network metrics in the chronic stage and the animals' epileptogenicity, here quantified as the number of iHPD (reminiscent of focal seizures) measured at the chronic stage.

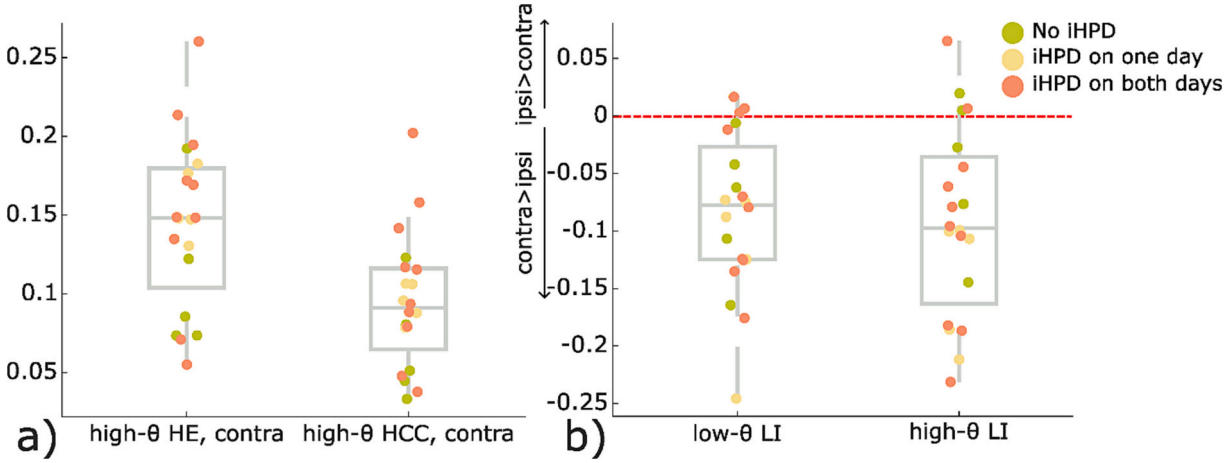

Fig. 6. Network metrics and iHPD measured at the chronic stage. A) Boxplots of high-theta HE and HCC averaged over d28 and d29; b) Boxplots of low-theta and high-theta LI, averaged over d28 and d29. The red dotted line represents the zero value, where the network is perfectly balanced between the two hemispheres. Each dot represents an animal, and it is colour-coded according to whether it showed iHPD on both days (red), only on one of the two days at chronic stage (yellow) or whether it showed no iHPD at all (green). (For interpretation of the references to colour in this figure legend, the reader is referred to the web version of this article.)

4. Discussion

We investigated brain network changes and their stability in a mouse model of TLE. We analyzed EEG segments from the recordings made before the hippocampal injection (d0) and segments free of epileptiform activities (EA) on two consecutive days at the chronic stage (d28 and d29). We found that: 1) the network becomes asymmetric in the theta frequency bands, with an increase of both integration and segregation of the contralateral hemisphere; 2) this asymmetry is stable and reproducible over consecutive days, and so are EA; 3) there is no correlation between network changes and the frequency of EA.

4.1. Brain network reorganization in the contralateral hemisphere

Using cross-correlation functions, we previously demonstrated that the functional connectivity (FC) networks become increasingly asymmetric during epileptogenesis in the KA mouse model, that interhemispheric FC is reduced and that nodes in the non-injected hemisphere become more important for driving network dynamics (Słowiński et al., 2019). We suggested an increased contribution of these nodes to the generation of EA in a self-sustained fashion, in line with results showing that silencing the injected hippocampus at the chronic stage does not control network IEDs (Sheybani et al., 2018). Our current results confirm these previous findings of increased asymmetry using a different group of animals and connectivity metric (PLI), suggesting strong replicability. Furthermore, we localize this asymmetry in the theta frequency bands (4–8 and 8–12 Hz): the network becomes lateralized toward the non-injected hemisphere which was significant at both d28 and d29 (see Fig. S4). The nodal strength (Supplementary Fig. S3) suggests that this lateralization might depend on two different mechanisms. While in high-theta it appears to be influenced solely by an increased strength of the nodes in the right hemisphere, in low-theta this lateralization is likely to be further boosted by a drop of strength of the nodes surrounding the injected hippocampus. A reduction in low-frequency network activity (4–8 Hz) in the injected hippocampus was already observed in the model (Dugladze et al., 2007). It is possible that this lateralization in two frequency bands reflects cell death on the injected side (4–8 Hz) and an independent evolution of EEG activity in the contralateral hippocampus (8–12 Hz) (Arabadzisz et al., 2005).

The concurrent contralateral increase of integration and segregation (HE and HCC respectively) suggests that the non-injected hemisphere tends to a stronger small-world organization (Humphries and Gurney, 2008) and is consistent with what was found in other animal studies and in humans. In a rodent TLE model in which KA was administered intraperitoneally, leading to more widespread epileptic alterations, increases in whole-brain GE, CC and small-worldness were found (Singh et al., 2017), which resembles what we found here for a more focal model of unilateral TLE (Lévesque and Avoli, 2016). It's worth noting that higher connectivity strength, GE and CC were found also in the latent phase of a intrahippocampal KA model (Li et al., 2021). In humans, higher GE (Carboni et al., 2020) and concurrent higher CC (Rigoni et al., 2023b) were found at the whole-brain level in spike-free interictal EEG segments of TLE patients. Contrarily to our results, in TLE patients, it is the ipsilateral hemisphere that shows higher HE and HCC (Rigoni et al., 2023b). The proportion between damaged and healthy tissue is presumably higher in the mouse model of TLE than in most of human patients and the hippocampal lesion is then likely to be more disruptive in mice than in humans, potentially explaining these different results. Species specificities in inter-hemispheric structural connectivity (Suárez et al., 2014) could also play a role. Moreover, our analyses were limited to the first 30 days after KA injection, while some patients undergo EEG examination after showing seizures for years. Therefore, it is unknown if the same network metric changes would be found in mice recorded over the long term, after several weeks or months. At the nodal level, we observed a significant increase of both local efficiency and CC around the non-injected hippocampus (see Fig. 4.a), further suggesting a strengthening of its independent role in driving brain activity at the chronic stage. *Comparison with other connectivity studies.*

Brain network studies in rodent models of TLE are rare, they employed various animal models and were mainly carried out using fMRI imaging. Studies involving intraperitoneal and intrahippocampal KA models report an increase of connectivity at the chronic stage (Bertoglio et al., 2019), accompanied by a whole-brain increase of CC, GE and small-world (Li et al., 2021; Singh et al., 2017). However, contradictory findings also exist that show lower integration and segregation and more time spent in states of lower connectivity at the chronic stage (Christiaen et al., 2019, 2020). As stated above, systemic injections are known for causing more widespread damage to subcortical structures and cerebral cortex (Lévesque and Avoli, 2016), potentially explaining why whole-brain network changes are observed, rather than only hemispheric changes (Bertoglio et al., 2019; Christiaen et al., 2019, 2020; Singh et al., 2017). Moreover, fMRI studies quantify FC from continuous data, during which the undocumented occurrence of spikes could have contributed to changes of FC.

4.2. Reproducibility of measures at the chronic stage

We demonstrate that not only the network topology (network metrics) is stable but also the functional connections that give rise to these metrics (PLI connectomes) are highly replicable at the chronic stage, suggesting that the increased theta-asymmetry of the network represents a distinct feature of the chronic stage. Indeed, on one side we don't find any difference between network metrics (global, hemispheric and nodal) and on the other we find excellent reliability of average connectomes at d28 and d29, at all frequency bands (ICC > 0.9, $p < .001$). While a lack of difference may not inherently indicate similarity, the high ICC values between connections confirms that the same underlying network is responsible for the comparable network metrics at d28 and d29. For further studies in rodent models of TLE, this suggests that EEG recordings lasting up to 15 days of chronic state (Samiee et al., 2018) may not be necessary for accurately characterizing the animals' brain network. However, given that we demonstrated here the stability of network metrics during the beginning of the chronic phase only, it would be interesting to investigate their evolution over months after KA injection. A possible way to do this would be to test periodically (e.g., every 7 days) animals during short recordings (e.g., 40 min) over two consecutive days.

We also demonstrate that most of the automatically identified EA, namely ictal hippocampal paroxysmal discharges (HPD), total number of fast ripples (FR), isolated FR, network IEDs and isolated spikes, are stable over consecutive days in the chronic state. The absence of reproducibility for short HPD and spike trains could be linked to the low number of events detected by the algorithm and the intrinsic variability of these epileptic activities. Altogether, this suggests that a 40-min epicranial EEG recording is adequate for quantifying epileptic activity in the intrahippocampal KA mouse model of TLE, which is a more feasible approach than implementing weeks-months of video-EEG monitoring (Li et al., 2021).

4.3. Absence of correlation with epileptic features

We did not find any significant correlation between those network metrics that changed at the chronic stage (contralateral HE, contralateral CC, LI) and EEG measures of epileptic activity. Given the high repeatability of these measures across consecutive days, we cannot attribute the absence of correlation to artefactual EEG data or to the inability to correctly characterize epilepsy severity.

Our results are in contrast with studies that found a clear positive correlation between seizure frequency and connectivity, GE and CC at chronic stage (Bertoglio et al., 2019; Christiaen et al., 2019, 2020; Samiee et al., 2018), suggesting a higher network synchrony is necessary for seizure generation. Considering that fMRI-derived networks are

reasonably affected by undocumented epileptiform discharges, the characteristics of these networks are likely to reflect networks' ability to not only *propagate* seizures but also *generate* epileptic activity. Here, however, we selected EEG epochs free from any EA and were therefore able to focus only on the resting-state, EA-free, network activity of epileptic animals.

Considering that network changes are robust over consecutive days, it seems reasonable to say they must represent some consistent systemic mechanism underlying interictal EA-free activity. It has been proposed that nodes in the contralateral hemisphere assume a pivotal role in the *propagation* of seizures and network IEDs (Sheybani et al., 2018; Słowiński et al., 2019). However, here we found no correlation between increased asymmetry and network IEDs, suggesting that the observed mechanism is a different one. It is possible that the detected changes in the contralateral network reflect inhibitory mechanisms that could be active during the interictal period free of EA analyzed here. In line with this interpretation, the absence of correlation between seizure frequency and the increased independence of the contralateral hippocampus (seen as loss of interhemispheric connectivity) was interpreted as evidence for a mechanism preventing seizure generalization (Arabadzisz et al., 2005). The importance of feedforward inhibition in restraining epileptiform events was already shown using in vitro models of epilepsy in acute rodent slices, so that a disruption of this inhibitory mechanism is necessary for seizure propagation (Trevelyan et al., 2006, 2007). The Interictal Suppression Hypothesis, according to which "the SOZ is actively suppressed by the rest of the brain", has also been put forward in humans (Johnson et al., 2023). Intracranial recordings showed that the SOZ has increased inward connectivity, suggesting the existence of an inhibitory network that actively silences the epileptic focus during spike-free interictal activity (Gunnarsdottir et al., 2021; Johnson et al., 2023; Narasimhan et al., 2020). This interpretation would also explain those failed attempts in humans to find a relationship between interictal connectivity and clinical variables such as seizure frequency or epilepsy duration (Carboni et al., 2020). Considering these results, we hypothesize that the emerging contralateral network might play an inhibitory or compensatory role or a mixture thereof, but future studies including also behavioral scores should be performed to untangle these potential effects. The lack of correlation is also an illustration of the concept that epilepsy cannot be reduced to the sole repetition of EA, or its correlated variables, but extends to impact independent networks.

4.4. Methodological considerations

Aside from the methodological considerations discussed above, another limitation of the current study comprises the absence of a saline-injected control group, to rule out the effect of animal ageing on network lateralization. Moreover, all animals should have ideally been collected at all three timepoints, to further test that the same differences (d0-d28) exist between d0 and d29. Nevertheless, the absence of significant differences between d28 and d29 in this retrospective analysis makes this last point less relevant. Finally, we had no long-term EEG monitoring to record potential seizures between d0 and d28 that may modulate the evolution in individual animals. Indeed, in 5 animals we did not record seizures neither at d28 nor at d29, which could suggest that they were still in the latent phase. However, considering that these animals show clear sign of *epi*leptic activity (see Supplementary Tables S1 and S2) and that they seem to belong to the same population of the other animals who show iHPD (see Fig. 6, where no specific cluster is visible), it is reasonable to think that the absence of seizure in these animals is mostly due to the short duration of the recordings rather to the animals not being in the chronic phase.

5. Conclusions

Altogether, we find that the role of the non-injected hemisphere becomes consistently more prominent in the network at the chronic epilepsy stage. However, the absence of correlation with epileptic activity does not allow us to determine whether this prominent contralateral network represents a network supporting propagation of epileptic activity or rather represents an inhibitory compensatory mechanism in response to focal epileptic activity.

CRediT authorship contribution statement

Isotta Rigoni: Conceptualization, Data curation, Formal analysis, Methodology, Project administration, Visualization, Writing – original draft, Writing – review & editing. **Guru Prasad Padmasola:** Data curation, Methodology, Visualization, Writing – original draft, Writing – review & editing. **Laurent Sheybani:** Data curation, Writing – review & editing. **Karl Schaller:** Funding acquisition, Writing – review & editing. **Charles Quairiaux:** Conceptualization, Funding acquisition, Investigation, Writing – original draft, Writing – review & editing. **Serge Vulliemoz:** Conceptualization, Funding acquisition, Investigation, Writing – original draft, Writing – review & editing.

Declaration of Competing Interest

SV is board member and shareholder of Epilog NV.

Data and materials availability

The raw data and the derivatives are available on Zenodo : 10.5281/zenodo.10227928.

The code used can be found at: https://github.com/IsottaR/ir_mice_project_Zenodo

Acknowledgement

This work was supported by Swiss National Science Foundation (SNSF) grant no. 192749 CRSII5_170873 and CRSII5_209470 to SV and grant no. 206720 to LS.

Appendix A. Supplementary data

Supplementary data to this article can be found online at https://doi.org/10.1016/j.nbd.2023.106382.

References

Arabadzisz, D., Antal, K., Parpan, F., Emri, Z., Fritschy, J.M., 2005. Epileptogenesis and chronic seizures in a mouse model of temporal lobe epilepsy are associated with distinct EEG patterns and selective neurochemical alterations in the contralateral hippocampus. Exp. Neurol. 194 (1), 76–90. https://doi.org/10.1016/j.expneurol.2005.01.029.

Arash Salarian, . ICC. Intraclass Correlation Coefficient (ICC). Https://Www.Mathworks.Com/Matlabcentral/Fileexchange/22099-Intraclass-Correlation-Coefficient-Icc. In: MATLAB Central File Exchange. Retrieved November 13, 2023.

Bartolomei, F., Lagarde, S., Wendling, F., McGonigal, A., Jirsa, V., Guye, M., Bénar, C., 2017. Defining epileptogenic networks: contribution of SEEG and signal analysis. Epilepsia 58 (7), 1131–1147. https://doi.org/10.1111/epi.13791.

Bertoglio, D., Jonckers, E., Ali, I., Verhoye, M., Van Der Linden, A., 2019. In vivo measurement of brain network connectivity reflects progression and intrinsic disease severity in a model of temporal lobe epilepsy. Neurobiol. Dis. 127, 45–52.

Carboni, M., Rubega, M., Iannotti, G.R., De Stefano, P., Toscano, G., Tourbier, S., Pittau, F., Hagmann, P., Momjian, S., Schaller, K., Seeck, M., Michel, C.M., van Mierlo, P., Vulliemoz, S., 2019. The network integration of epileptic activity in relation to surgical outcome. Clin. Neurophysiol. 130 (12), 2193–2202. https://doi.org/10.1016/j.clinph.2019.09.006.

Carboni, M., De Stefano, P., Vorderwülbecke, B.J., Tourbier, S., Mullier, E., Rubega, M., Momjian, S., Schaller, K., Hagmann, P., Seeck, M., Michel, C.M., van Mierlo, P., Vulliemoz, S., 2020. Abnormal directed connectivity of resting state networks in focal epilepsy. NeuroImage Clin. 27 (July), 102336 https://doi.org/10.1016/j.nicl.2020.102336.

Christiaen, E., Goossens, M., Raedt, R., Descamps, B., Emil, L., Craey, E., Carrette, E., Vonck, K., Boon, P., Vanhove, C., 2019. Alterations in the functional brain network in a rat model of epileptogenesis: a longitudinal resting state fMRI study. NeuroImage 202 (March), 116144. https://doi.org/10.1016/j.neuroimage.2019.116144.

Christiaen, E., Goossens, M.G., Descamps, B., Larsen, L.E., Boon, P., Raedt, R., Vanhove, C., 2020. Dynamic functional connectivity and graph theory metrics in a rat model of temporal lobe epilepsy reveal a preference for brain states with a lower functional connectivity, segregation and integration. Neurobiol. Dis. 139 (December 2019), 104808 https://doi.org/10.1016/j.nbd.2020.104808.

Coito, A., Plomp, G., Genetti, M., Abela, E., Wiest, R., Seeck, M., Michel, C.M., Vulliemoz, S., 2015. Dynamic directed interictal connectivity in left and right temporal lobe epilepsy. Epilepsia 56 (2), 207–217. https://doi.org/10.1111/epi.12904.

Coito, A., Michel, C.M., Vulliemoz, S., Plomp, G., 2019. Directed functional connections underlying spontaneous brain activity. Hum. Brain Mapp. 40 (3), 879–888. https://doi.org/10.1002/hbm.24418.

de Campos, B.M., Coan, A.C., Lin Yasuda, C., Casseb, R.F., Cendes, F., 2016. Large-scale brain networks are distinctly affected in right and left mesial temporal lobe epilepsy. Hum. Brain Mapp. 37 (9), 3137–3152. https://doi.org/10.1002/hbm.23231.

Dugladze, T., Vida, I., Tort, A.B., Gross, A., Otahal, J., Heinemann, U., Kopell, N.J., Gloveli, T., 2007. Impaired hippocampal rhythmogenesis in a mouse model of mesial temporal lobe epilepsy. Proc. Natl. Acad. Sci. U. S. A. 104 (44), 17530–17535. https://doi.org/10.1073/pnas.0708301104.

Fisher, R.S., Acevedo, C., Arzimanoglou, A., Bogacz, A., Cross, J.H., Elger, C.E., Engel, J., Forsgren, L., French, J.A., Glynn, M., Hesdorffer, D.C., Lee, B.I., Mathern, G.W., Moshé, S.L., Perucca, E., Scheffer, I.E., Tomson, T., Watanabe, M., Wiebe, S., 2014. ILAE official report: a practical clinical definition of epilepsy. Epilepsia 55 (4), 475–482. https://doi.org/10.1111/epi.12550.

Geut, I., Weenink, S., Knottnerus, I.L.H., van Putten, M.J.A.M., 2017. Detecting interictal discharges in first seizure patients: ambulatory EEG or EEG after sleep deprivation? Seizure 51, 52–54. https://doi.org/10.1016/j.seizure.2017.07.019.

Gunnarsdottir, K.M., Li, A., Smith, R.J., Kang, J.-Y., Korzeniewska, A., Crone, N.E., Rouse, A.G., Cheng, J.J., Kinsman, M.J., Landazuri, P., Uysal, U., Ulloa, C.M., Cameron, N., Cajigas, I., Jagid, J., Kanner, A., Elarjani, T., Bicchi, M.M., Inati, S., Sarma, S.V., 2021. Source-sink connectivity: a novel interictal EEG marker for seizure localization. Brain 145 (11). https://doi.org/10.1093/brain/awac300, 2021.10.15.464594.

Humphries, M.D., Gurney, K., 2008. Network "small-world-ness": a quantitative method for determining canonical network equivalence. PLoS One 3 (4). https://doi.org/10.1371/journal.pone.0002051.

Johnson, G.W., Doss, D.J., Morgan, V.L., Paulo, D.L., Cai, L.Y., Shless, J.S., Negi, A.S., Gummadavelli, A., Kang, H., Reddy, S.B., Naftel, R.P., Bick, S.K., Roberson, S.W., Dawant, B.M., Wallace, M.T., Englot, D.J., 2023. The Interictal suppression hypothesis in focal epilepsy: network-level supporting evidence. Brain 146 (7), 2828–2845. https://doi.org/10.1093/brain/awad016.

Kay, B.P., Difrancesco, M.W., Privitera, M.D., Gotman, J., Holland, S.K., Szaflarski, J.P., 2013. Reduced default mode network connectivity in treatment-resistant idiopathic generalized epilepsy. Epilepsia 54 (3), 461–470. https://doi.org/10.1111/epi.12057.

King, M.A., Newton, M.R., Jackson, G.D., Fitt, G.J., Mitchell, L.A., Silvapulle, M.J., Berkovic, S.F., 1998. Epileptology of the first-seizure presentation: a clinical, electroencephalographic, and magnetic resonance imaging study of 300 consecutive patients. Lancet 352 (9133), 1007–1011. https://doi.org/10.1016/S0140-6736(98)03543-0.

Latora, V., Marchiori, M., 2001. Efficient behavior of small-world networks. Phys. Rev. Lett. 87 (19) https://doi.org/10.1103/PhysRevLett.87.198701, 198701-1-198701–198704.

Lévesque, M., Avoli, M., 2016. The kainic acid model of temporal lobe epilepsy. Neurosci. Biobehav. Rev. 37, 2887–2899. https://doi.org/10.1016/j.neubiorev.2013.10.011.The.

Lévesque, M., Salami, P., Shiri, Z., Avoli, M., 2018. Interictal oscillations and focal epileptic disorders. Eur. J. Neurosci. 48 (8), 2915–2927. https://doi.org/10.1111/ejn.13628.

Li, L., He, L., Harris, N., Zhou, Y., Engel, J., Bragin, A., 2021. Topographical reorganization of brain functional connectivity during an early period of epileptogenesis. Epilepsia 62 (5), 1231–1243. https://doi.org/10.1111/epi.16863.

Lisgaras, C.P., Scharfman, H.E., 2022. Robust chronic convulsive seizures, high frequency oscillations, and human seizure onset patterns in an intrahippocampal kainic acid model in mice. Neurobiol. Dis. 166, 105637 https://doi.org/10.1016/j.nbd.2022.105637.

McGraw, K.O., Wong, S.P., 1996. "Forming inferences about some intraclass correlations coefficients": correction. Psychol. Methods 1 (4), 390. https://doi.org/10.1037//1082-989x.1.4.390.

Mégevand, P., Quairiaux, C., Lascano, A.M., Kiss, J.Z., Michel, C.M., 2008. A mouse model for studying large-scale neuronal networks using EEG mapping techniques. NeuroImage 42 (2), 591–602. https://doi.org/10.1016/j.neuroimage.2008.05.016.

Narasimhan, S., Kundassery, K.B., Gupta, K., 2020. Seizure-onset regions demonstrate high inward directed connectivity during resting-state: an SEEG study in focal epilepsy. Epilepsia 61 (11), 2534–2544. https://doi.org/10.1111/epi.16686.Seizure-onset.

Oostenveld, R., Fries, P., Maris, E., Schoffelen, J.M., 2011. FieldTrip: open source software for advanced analysis of MEG, EEG, and invasive electrophysiological data. Comput. Intell. Neurosci. 2011 https://doi.org/10.1155/2011/156869.

Paschen, E., Elgueta, C., Heining, K., Vieira, D.M., Kleis, P., Orcinha, C., Häussler, U., Bartos, M., Egert, U., Janz, P., Haas, C.A., 2020. Hippocampal low-frequency stimulation prevents seizure generation in a mouse model of mesial temporal lobe epilepsy. ELife 9, 1–57. https://doi.org/10.7554/ELIFE.54518.

Perrin, F., Pernier, J., Bertrand, O., 1989. Spherical splines for scalp potential and current density mapping. Electroencephalogr. Clin. Neurophysiol. 72, 184–187.

Quairiaux, C., Mégevad, P., Kiss, J.Z., Michel, C.M., 2011. Functional development of large-scale sensorimotor cortical networks in the brain. J. Neurosci. 31 (26), 9574–9584. https://doi.org/10.1523/JNEUROSCI.5995-10.2011.

Racine, R.J., 1972. Modification of seizure activity by electrical stimulation. II. Motor seizure. Electroencephalogr. clin. neurophysiol. 32, 281–294. https://doi.org/10.1016/0013-4694(72)90177-0.

Riban, V., Bouilleret, V., Pham-le, B.T., Fritschy, J.M., Marescaux, C., Depaulis, A., 2002. Evolution of hippocampal epileptic activity during the development of hippocampal sclerosis in a mouse model of temporal lobe epilepsy. Neuroscience 112 (7), 101–111.

Rigoni, I., Rué Queralt, J., Glomb, K., Preti, M.G., Roehri, N., Tourbier, S., Spinelli, L., Seeck, M., Van De Ville, D., Hagmann, P., Vulliémoz, S., 2023a. Structure-function coupling increases during interictal spikes in temporal lobe epilepsy: a graph signal processing study. Clin. Neurophysiol. 153, 1–10. https://doi.org/10.1016/j.clinph.2023.05.012.

Rigoni, I., Vorderwülbecke, B., Carboni, M., Roehri, N., Spinelli, L., Tononi, G., Seeck, M., Perogamvros, L., Vulliémoz, S., 2023b. Network alterations in temporal lobe epilepsy during non-rapid eye movement sleep and wakefulness. MedRxiv 1–20. https://doi.org/10.1101/2023.10.06.23296655.

Rubinov, M., Sporns, O., 2010. Complex network measures of brain connectivity: uses and interpretations. NeuroImage 52 (3), 1059–1069. https://doi.org/10.1016/j.neuroimage.2009.10.003.

Rusina, E., Bernard, C., Williamson, A., 2021. The kainic acid models of temporal lobe epilepsy. ENeuro 8 (2). https://doi.org/10.1523/ENEURO.0337-20.2021.

Samiee, S., Lévesque, M., Avoli, M., Baillet, S., 2018. Phase-amplitude coupling and epileptogenesis in an animal model of mesial temporal lobe epilepsy. Neurobiol. Dis. 114 (October 2017), 111–119. https://doi.org/10.1016/j.nbd.2018.02.008.

Sharma, S., Puttachary, S., Thippeswamy, A., Kanthasamy, A.G., Thippeswamy, T., 2018. Status Epilepticus: Behavioral and Electroencephalography Seizure Correlates in Kainate Experimental Models. Front Neurol. 1–8. https://doi.org/10.3389/fneur.2018.00007.

Sheybani, L., Birot, G., Contestabile, A., Seeck, M., Kiss, J.Z., Schaller, K., Michel, C.M., Quairiaux, C., 2018. Electrophysiological evidence for the development of a self-sustained large-scale epileptic network in the kainate mouse model of temporal lobe epilepsy. J. Neurosci. 38 (15), 3776–3791. https://doi.org/10.1523/JNEUROSCI.2193-17.2018.

Sheybani, L., Van Mierlo, P., Birot, G., Michel, C.M., 2019. Large-Scale 3–5 Hz Oscillation Constrains the Expression of Neocortical Fast-Ripples in a Mouse Model of Mesial Temporal Lobe Epilepsy.

Silachev, D., Koval, A., Savitsky, M., Padmasola, G., Quairiaux, C., Thorel, F., Katanaev, V.L., 2022. Mouse models characterize GNAO1 encephalopathy as a neurodevelopmental disorder leading to motor anomalies: from a severe G203R to a milder C215Y mutation. Acta Neuropathol. Commun. 10 (1), 1–17. https://doi.org/10.1186/s40478-022-01312-z.

Singh, R., Mirsattari, S.M., Leung, L.S., 2017. Resting state functional network disruptions in a kainic acid model of temporal lobe epilepsy. NeuroImage Clin. 13, 70–81. https://doi.org/10.1016/j.nicl.2016.11.002.

Slinger, G., Otte, W.M., Braun, K.P.J., van Diessen, E., 2021. An updated systematic review and meta-analysis of brain network organization in focal epilepsy: looking back and forth. Neurosci. Biobehav. Rev. https://doi.org/10.1016/j.neubiorev.2021.11.028.

Słowiński, P., Sheybani, L., Michel, C.M., Richardson, M.P., Quairiaux, C., Terry, J.R., Goodfellow, M., 2019. Background EEG connectivity captures the time-course of epileptogenesis in a mouse model of epilepsy. ENeuro 6 (4). https://doi.org/10.1523/ENEURO.0059-19.2019.

Suárez, R., Gobius, H., Richards, L.J., 2014. Evolution and development of interhemispheric connections in the vertebrate forebrain. Front. Hum. Neurosci. 8 (JULY), 1–14. https://doi.org/10.3389/fnhum.2014.00497.

Terry, J.R., Benjamin, O., Richardson, M.P., 2012. Seizure generation: the role of nodes and networks. Epilepsia 53 (9), 166–169. https://doi.org/10.1111/j.1528-1167.2012.03560.x.

Trevelyan, A.J., Sussillo, D., Watson, B.O., Yuste, R., 2006. Modular propagation of epileptiform activity: evidence for an inhibitory veto in neocortex. J. Neurosci. 26 (48), 12447–12455. https://doi.org/10.1523/JNEUROSCI.2787-06.2006.

Trevelyan, A.J., Sussillo, D., Yuste, R., 2007. Feedforward inhibition contributes to the control of epileptiform propagation speed. J. Neurosci. 27 (13), 3383–3387. https://doi.org/10.1523/JNEUROSCI.0145-07.2007.

van Mierlo, P., Höller, Y., Focke, N.K., Vulliemoz, S., 2019. Network perspectives on epilepsy using EEG/MEG source connectivity. Front. Neurol. 10 (July), 1–13. https://doi.org/10.3389/fneur.2019.00721.

Verhoeven, T., Coito, A., Plomp, G., Thomschewski, A., Pittau, F., Trinka, E., Wiest, R., Schaller, K., Michel, C., Seeck, M., Dambre, J., Vulliemoz, S., van Mierlo, P., 2018. Automated diagnosis of temporal lobe epilepsy in the absence of interictal spikes. NeuroImage Clin. 17 (July 2017), 10–15. https://doi.org/10.1016/j.nicl.2017.09.021.

Watts, D.J., Strogatz, S.H., 1998. Collective dynamics of 'small-world' networks. Nature 393 (June), 440–442. https://www.ncbi.nlm.nih.gov/pubmed/9623998.

Weiss, S.A., Orosz, I., Salamon, N., Moy, S., Wei, L., Van't Klooster, M.A., Knight, R.T., Harper, R.M., Bragin, A., Fried, I., Engel Jr., J., Staba, R., 2016. Ripples on spikes show increased phase-amplitude coupling in mesial temporal lobe epilepsy. Epilepsia 57 (11), 1916–1930.

Wirrell, E.C., 2010. Prognostic significance of interictal epileptiform discharges in newly diagnosed seizure disorders. J. Clin. Neurophysiol. 27 (4), 239–248. https://doi.org/10.1097/WNP.0b013e3181ea4288.